SUPPLEMENTAL ONLINE MATERIAL FOR:

Deficient α5* nicotinic receptor signaling increases vulnerability to nicotine addiction

Christie D. Fowler[1], Qun Lu[1], Paul M. Johnson[1], Michael J. Marks[2] and Paul J. Kenny[1]

[1]Laboratory for Behavioral and Molecular Neuroscience, Department of Molecular Therapeutics, The Scripps Research Institute – Scripps Florida, Jupiter, FL 33458, USA;
[2]Institute of Behavioral Genetics, University of Colorado, Boulder, CO 80309, USA.

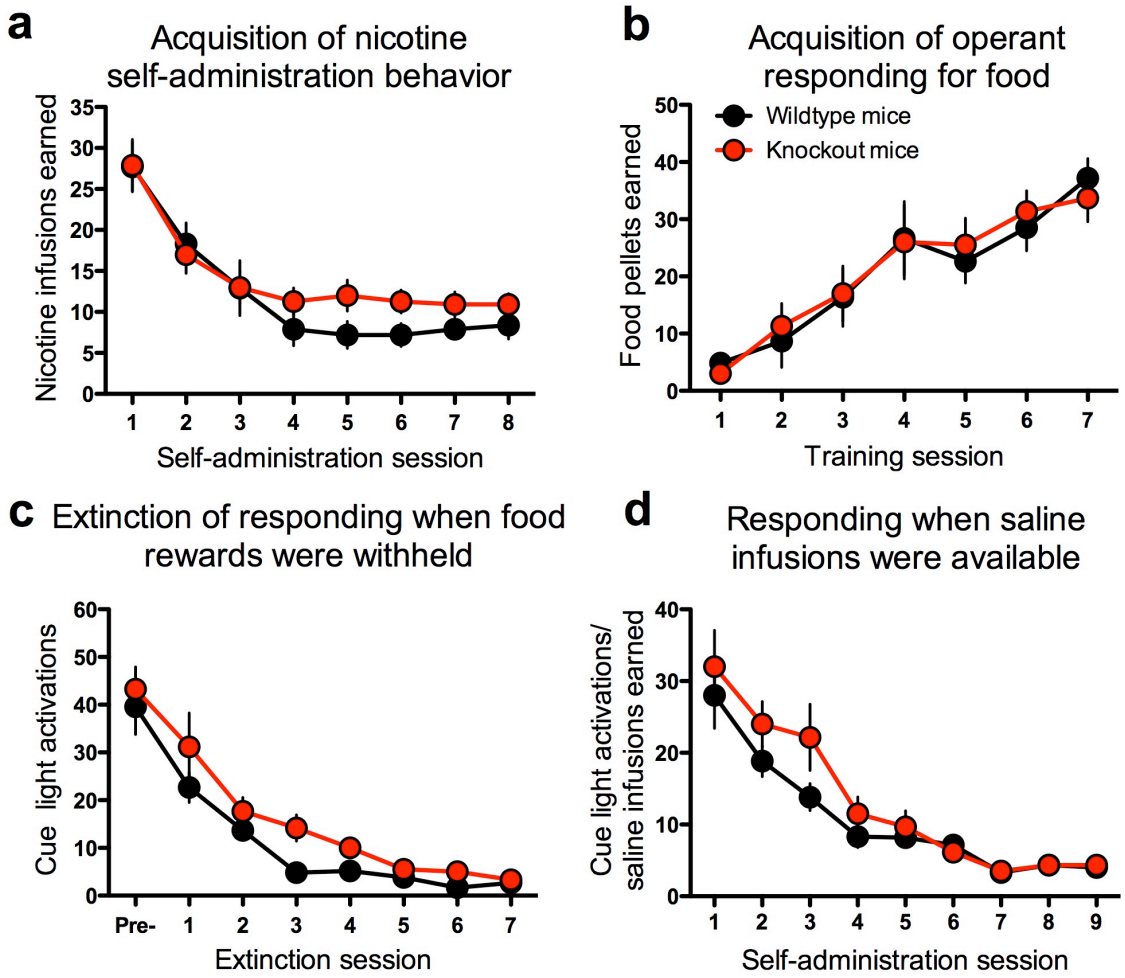

Supplementary Figure 1 | Operant responding for food or nicotine in wildtype and α5 knockout mice. (a) Wildtype and α5 knockout mice acquired stable intravenous nicotine self-administration behavior at the initial training dose (0.03 mg/kg/infusion; free-base) under a FR5TO20 sec schedule of reinforcement during 1 hour daily sessions (n=10-11/group). Data are presented as mean (± SEM) number of infusions earned for the 'active' lever. Two-way ANOVA, *Genotype* $F_{(1,133)}$=1.21, n.s.; *Day* $F_{(7,133)}$=29.02, p<0.0001; *Interaction* $F_{(7,133)}$=0.79, n.s. **(b)** Wildtype and α5 knockout mice (n=6/group) learned to lever press for food rewards on a FR5TO20 sec schedule of reinforcement during 1 hr daily sessions. Data are presented as mean ± SEM number of food rewards earned. Two-way ANOVA, *Genotype* $F_{(1,60)}$=0.01, n.s.; *Day* $F_{(6,60)}$=23.06, p<0.001; *Interaction* $F_{(6,60)}$=0.29, n.s. **(c)** After stable levels of food responding were established the food-paired cue light continued to be activated but food rewards were withheld following completion of the response criteria. Data are presented as mean ± SEM number of cue light activations earned. The last day of access to food is designated "Pre-". Two-way ANOVA, *Genotype* $F_{(1,80)}$=2.14, n.s.; *Day* $F_{(7,80)}$=68.98, p<0.0001; *Interaction* $F_{(7,80)}$=0.85, n.s. **(d)** Wildtype and α5 knockout mice failed to sustain self-administration behavior when intravenous infusions of nicotine were replaced with saline (n=6/group). Data are presented as mean (± SEM) number of infusions earned for the 'active' lever. Two-way ANOVA, *Genotype* $F_{(1,80)}$=1.46, n.s..; *Day* $F_{(8,80)}$=37.23, p<0.0001; *Interaction* $F_{(8,80)}$=0.97, n.s.

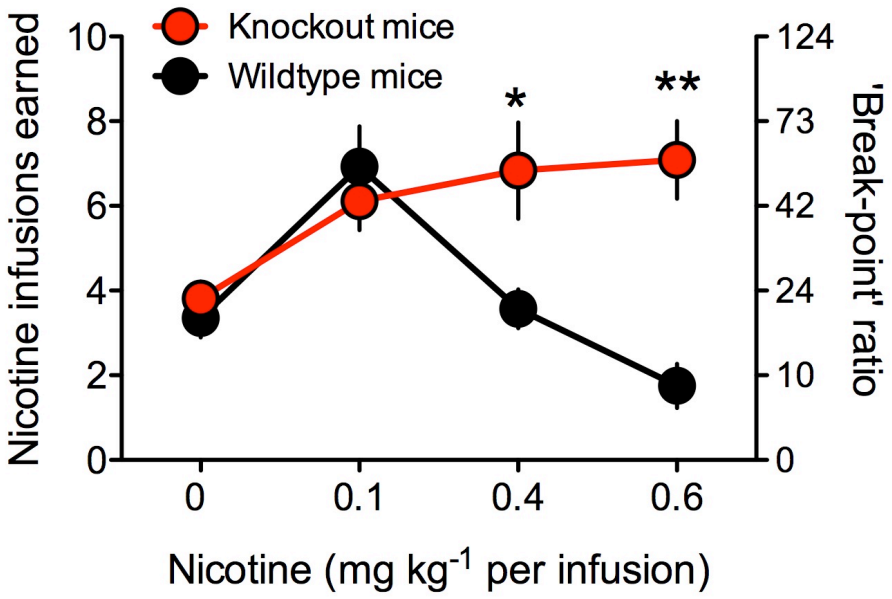

Supplementary Figure 2 | Nicotine self-administration in mice under a progressive ratio schedule of reinforcement. Data are presented as mean (± SEM) number of nicotine infusions earned and maximal number of lever presses emitted to obtain each given dose ('break-point' ratio). *Genotype* $F_{(1,49)}$=12.68, p<0.001; *Dose* $F_{(3,49)}$=5.22, p<0.01; *Interaction* $F_{(3,49)}$=5.36, p<0.01. *P<0.05, **p<0.01 and ***p<0.001 indicate statistically significant differences between genotypes at the indicated nicotine dose; post-tests after significant interaction effects; *n*=7-9 per group.

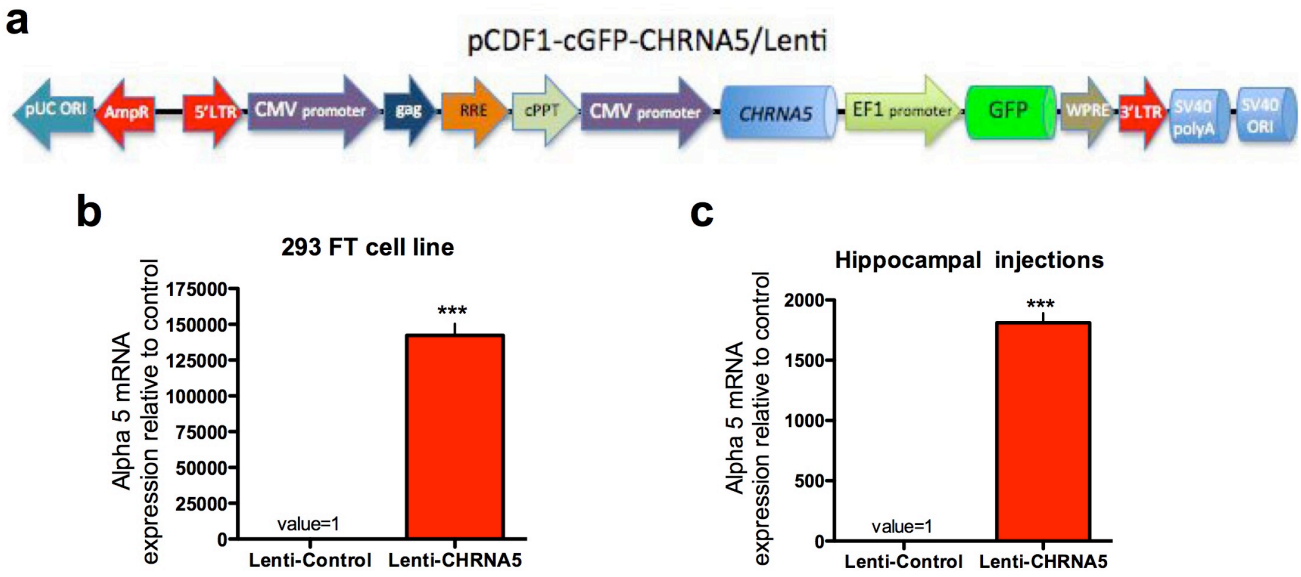

Supplementary Figure 3 | Validation of the Lenti-CHRNA5 re-expression vector for mice. (a) Lentivirus vector map detailing construct. **(b)** Real-time PCR analysis of α5 nAChR mRNA in 293 FT cells 24 hr post-transfection of the Lenti-Control or Lenti-CHRNA5 expression construct. Data are presented as mean (± SEM) fold change compared to the untransfected control mean (method of $2^{-\Delta\Delta CT}$); ***$t_{(4)}$=17.57, p<0.001. **(c)** Real-time RT-PCR analysis of α5 nAChR subunit mRNA expression in α5 knockout mice injected with Lenti-Control or Lenti-CHRNA5 virus into the hippocampus. Mice were euthanized ≥ 3 weeks after injection, and hippocampal microdissections were performed. Data are presented as mean (± SEM) fold change compared to the control mean (method of $2^{-\Delta\Delta CT}$); $t_{(3)}$=17.42, ***p<0.001 versus control.

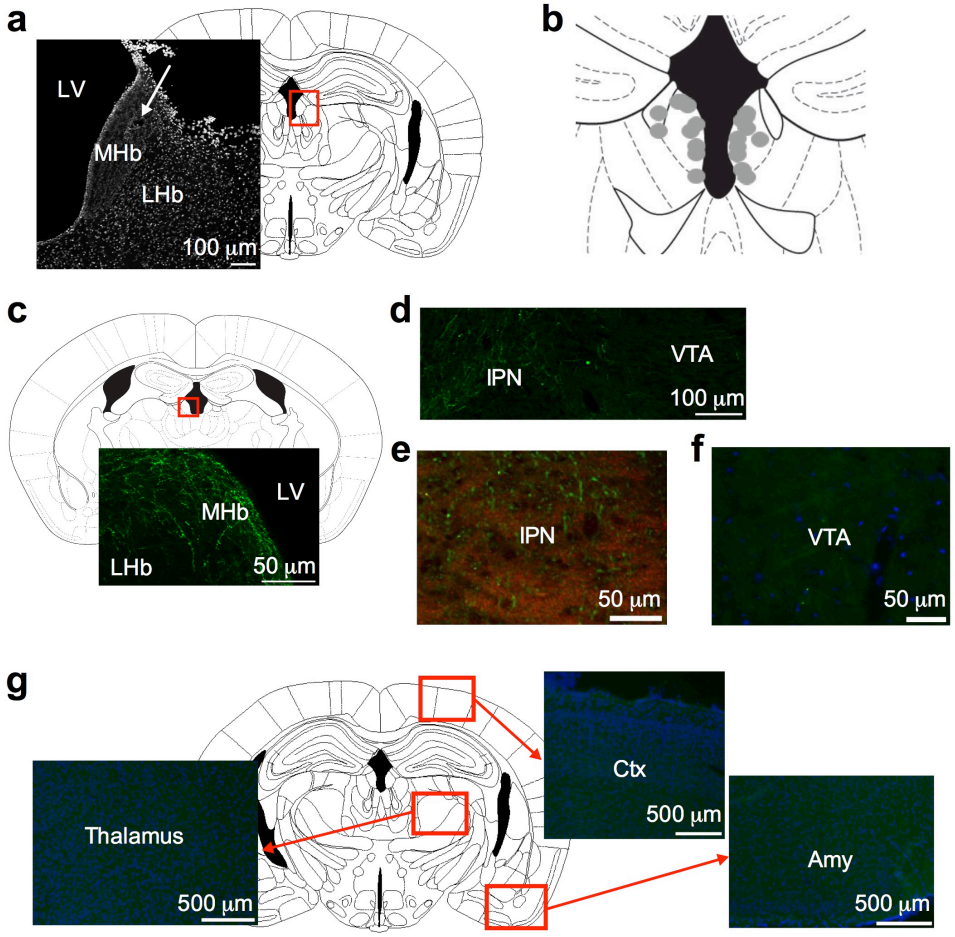

Supplementary Figure 4 | Additional images from lentivirus-injected mouse brains. (a) Photomicrograph showing injection site in the MHb of the mouse. The mouse was injected two weeks prior to being euthanized, allowing for visualization of the injection tract. The tissue is labeled with DAPI. The schematic diagram illustrates area visualized (red box). Scale bar = 100 μm. LHb: lateral habenula; LV: lateral ventricle. **(b)** Schematic diagram depicting site of highest density of GFP-labeled cells in control and knockout mice injected with the Lenti-CHRNA5 in the self-administration experiment. **(c)** Image displays GFP-labeled (green) cells and axons in the MHb several months following the lentivirus injection. The schematic diagram illustrates area visualized (red box). The vast majority of labeled axons were restricted to the MHb, with very few detected in LHb. This low-level LHb staining may represent axonal projections from the MHb known to pass through the LHb to the fasciculus retroflexus, or limited spread of virus to LHb. Scale bar = 50 μm. **(d)** Image displays GFP-labeled axons in the IPN following lentiviral injection in the MHb several months prior. The brain section was cut at an angle to allow visualization of axons entering the IPN, although labeled axons may also represent limited MHb innervation of the interfascicular nucleus. Few labeled axons were visualized in the VTA. Scale bar = 100 μm. **(e)** In the IPN, GFP-labeled axons were visualized four weeks following lentiviral injection in the MHb. The tissue is counterstained with VACHT (red) to verify localization within the IPN. Scale bar = 50 μm. **(f)** Image displays lack of GFP-labeling in the VTA following lentiviral injection in the MHb four weeks prior. Tissue counterstained with DAPI. Scale bar = 50 μm. **(g)** Control brain regions verify absence of viral spread as determined by GFP and DAPI staining from a mouse injected with lentivirus into the MHb four weeks prior. The schematic diagram illustrates the areas visualized (red box). Ctx: cortex; Amy: amygdala. Scale bars = 500 μm.

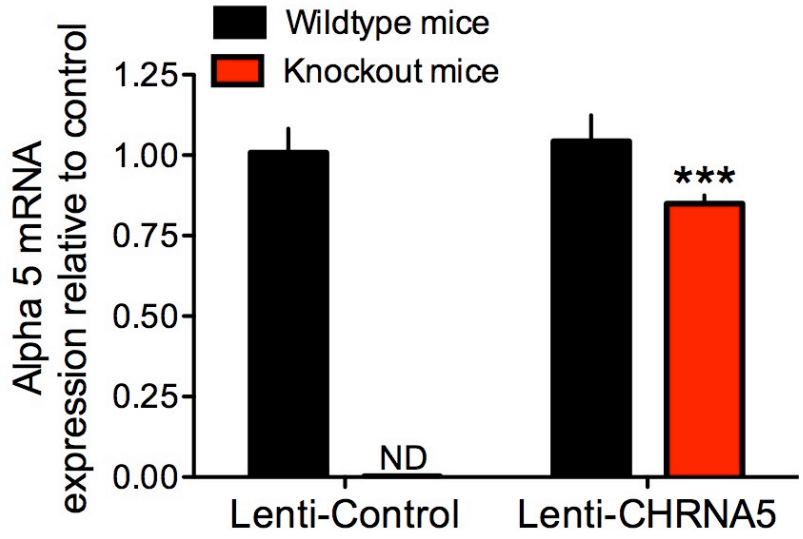

Supplementary Figure 5 | Rescue of α5 nAChR subunits in the MHb of lentivirus-injected knockout mice. Real time PCR analysis of α5 subunit mRNA expression was carried out in brain tissues from nicotine self-administering mice not used for GFP immunostaining (n=2-4 per group) (See panels c and d of Fig. 2 in main manuscript). Data are presented as mean (± SEM) fold change compared to the wildtype control Lenti-Control group mean (method of $2^{-\Delta\Delta CT}$). Two-way ANOVA: *Genotype* $F_{(1,8)}$=187.8, p<0.0001; *Lentivirus* $F_{(1,8)}$=104.2, p<0.0001; *Interaction* $F_{(1,8)}$=85.39, p<0.0001.

a

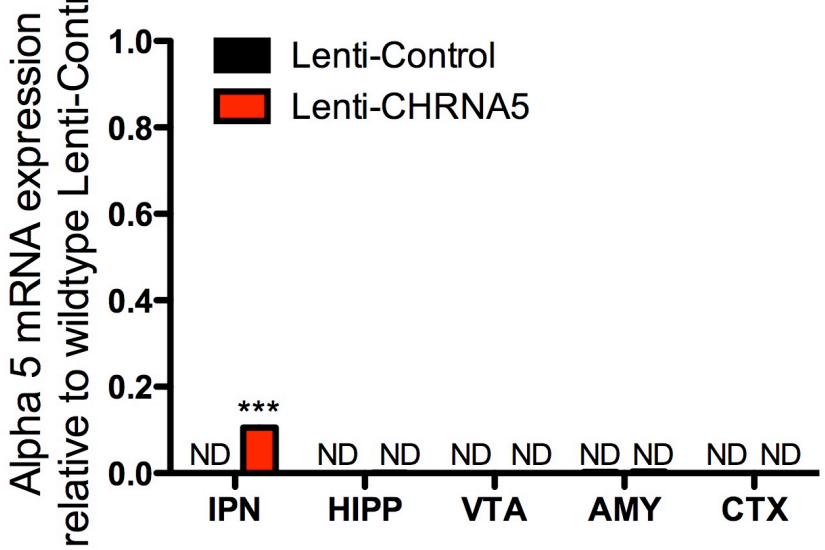

b

Habenular Injections

Mean ct values

Habenula	Alpha 5	β-Actin
WT Lenti-Control	26.26423	18.10296
WT Lenti-CHRNA5	26.21434	17.96892
KO Lenti-Control	34.86446	17.99476
KO Lenti-CHRNA5	26.94691	18.05849

IPN	Alpha 5	β-Actin
WT Lenti-Control	21.48007	19.84203
KO Lenti-Control	37.94406	22.8676
KO Lenti-CHRNA5	27.8756	22.98321

Hippocampus	Alpha 5	β-Actin
WT Lenti-Control	23.55759	17.72681
KO Lenti-Control	34.85867	18.06704
KO Lenti-CHRNA5	32.48013	17.52897

VTA	Alpha 5	β-Actin
WT Lenti-Control	22.65976	18.40449
KO Lenti-Control	35.80058	18.96847
KO Lenti-CHRNA5	34.89654	18.70205

Amygdala	Alpha 5	β-Actin
WT Lenti-Control	26.48075	18.2176
KO Lenti-Control	35.40989	18.92115
KO Lenti-CHRNA5	34.48429	18.04507

Cortex	Alpha 5	β-Actin
WT Lenti-Control	23.46124	18.078
KO Lenti-Control	35.41993	18.20996
KO Lenti-CHRNA5	34.80369	17.8422

Supplementary Figure 6 | α5 nAChR mRNA expression in control brain areas of mice following lentivirus injection. Mice were injected with the Lenti-Control or Lenti-CHRNA5 vector into the MHb. After an incubation period of ≥ three weeks, microdissections were performed of the IPN, hippocampus (HIPP; dorsal to the injection site), VTA, amygdala (AMY), and parietal cortex (CTX; dorsal to the injection site). ND: not detectable. **(a)** Data are presented as mean (± SEM) fold change compared to the wildtype control virus mean (method of $2^{-\Delta\Delta CT}$). IPN: $t_{(4)}$=72.52, p<0.001; HIPP: $t_{(4)}$=1.05, n.s.; VTA: $t_{(4)}$=0.03, n.s.; AMY: $t_{(4)}$=0.27, n.s.; CTX: $t_{(4)}$=0.07, n.s. ***P<0.001 compared to the α5 knockout Lenti-Control brain sample. **(b)** Data are presented as mean raw Ct values from the real-time RT-PCR for the α5 assay and representative β-actin loading control in wildtype (WT) and α5 knockout (KO) mice.

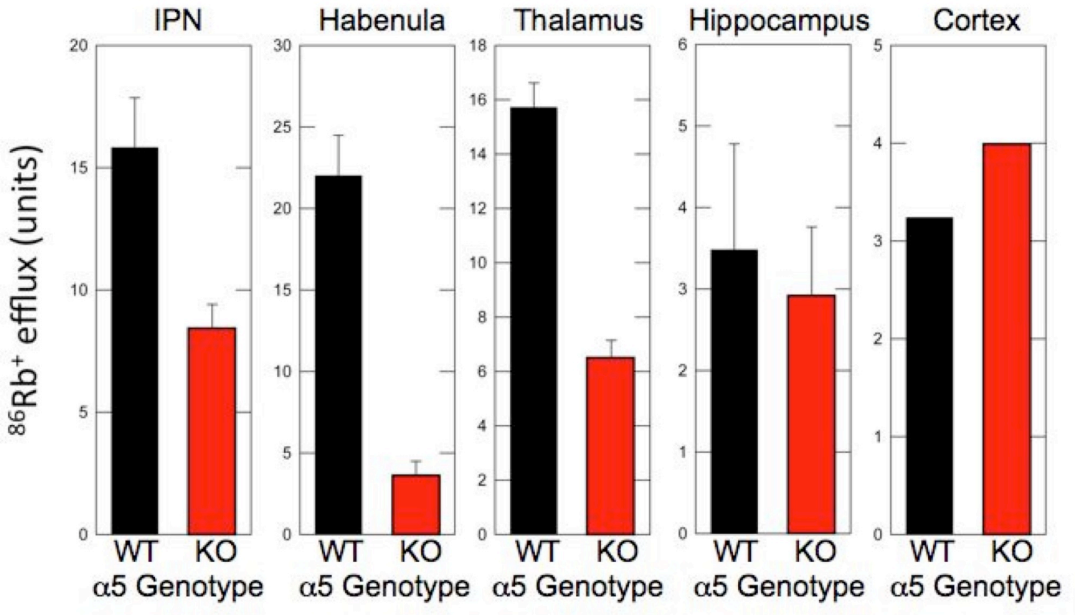

Supplementary Figure 7 | $^{86}Rb^+$ efflux from synaptosomes derived from α5 knockout mice. Acetylcholine-evoked $^{86}Rb^+$ efflux from the brains of wildtype and knockout mice. $^{86}Rb^+$ efflux was stimulated by a low (30 μM) concentration of acetylcholine. Data are presented as the mean (± SEM).

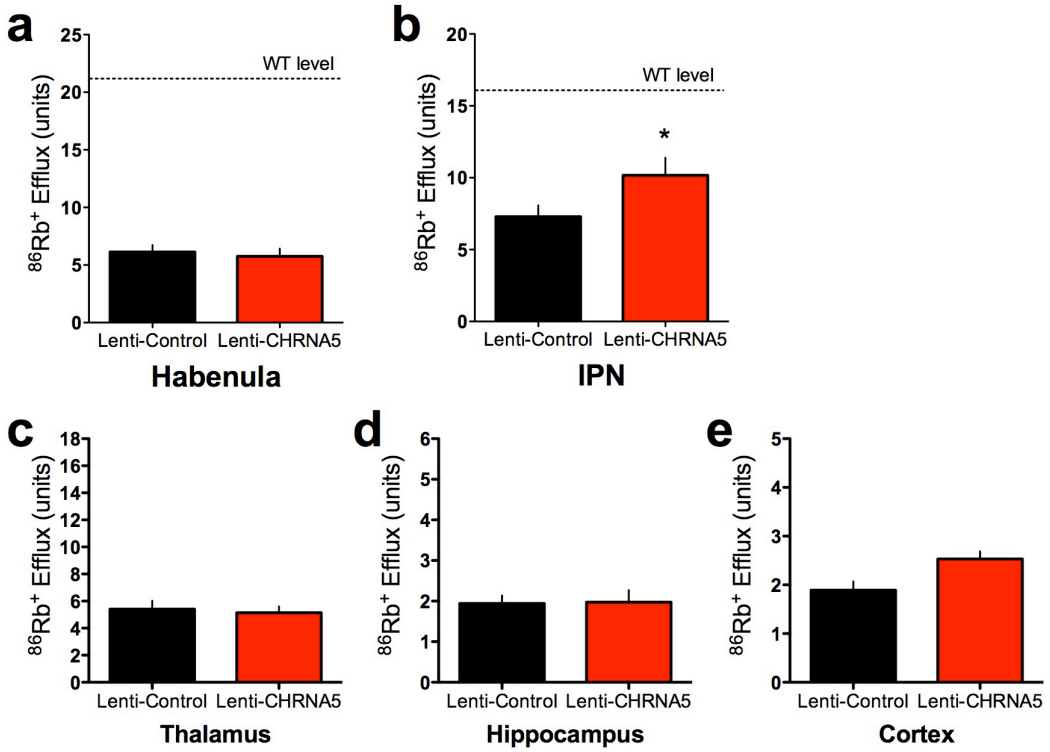

Supplementary Figure 8 | $^{86}Rb^+$ efflux from synaptosomes derived from α5 knockout mice. Acetylcholine-evoked $^{86}Rb^+$ efflux from the brains of wildtype and knockout mice. $^{86}Rb^+$ efflux in the habenula **(a)** and IPN **(b)** of α5 knockout mice previously treated with the Lenti-Control or Lenti-CHRNA5 virus in the MHb. $^{86}Rb^+$ efflux was stimulated by a low (30 μM) concentration of acetylcholine. Data are presented as the mean (± SEM). *Habenula*: T-test, $t_{(13)}$=0.41, n.s.; *IPN*: T-test, $t_{(13)}$=2.08, p<0.05.; *n*=6-9 per group**.** Deficits in $^{86}Rb^+$ efflux were unaltered in synaptosomes derived from the thalamus **(c)**, hippocampus **(d)** or cortex **(e)** of these mice. $^{86}Rb^+$ efflux was stimulated by a low (30μM) concentration of acetylcholine. Data are presented as the mean (± SEM).

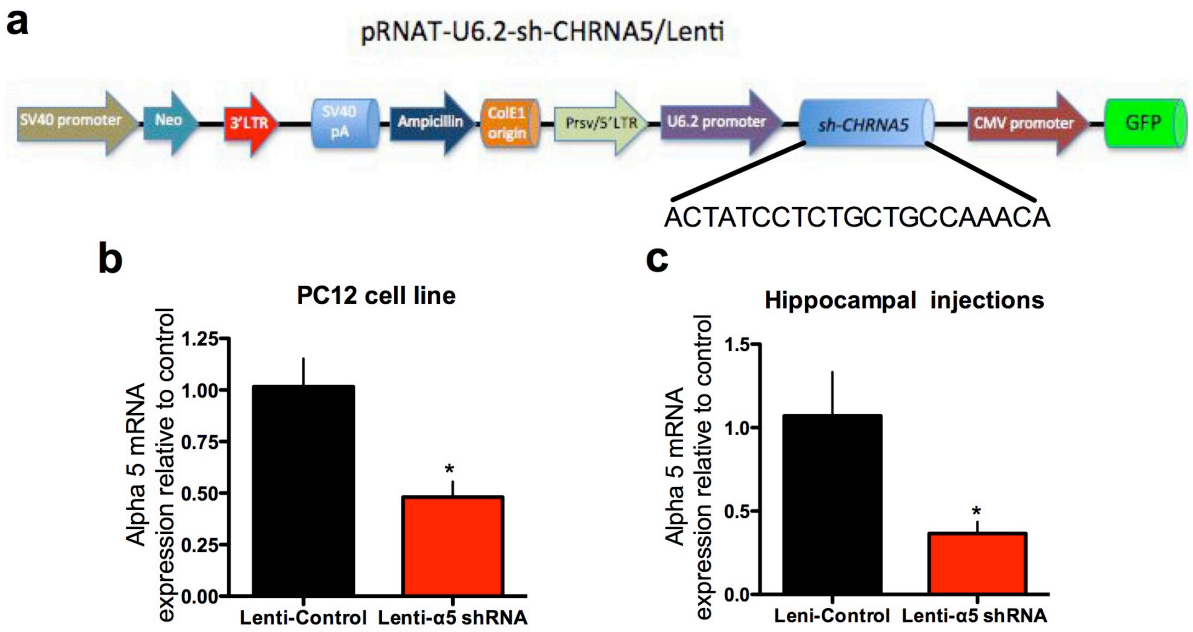

d

Habenular injections		
Mean ct values	Alpha 5	β-Actin
Lenti-Control	29.2273	18.4663
Lenti-α5 shRNA	30.3982	17.9833

Supplementary Figure 9 | Validation of Lenti-α5-shRNA knockdown vector for rats. (a) Lentivirus vector map detailing construct. **(b)** Real-time PCR data for α5 subunit mRNA in PC12 cells at 24 hr post-transfection of the Lenti-Control or Lenti-α5-shRNA expression vector. Data are presented as mean (± SEM) fold change compared to the untransfected control mean (method of $2^{-\Delta\Delta CT}$); $t_{(4)}=3.44$, $p<0.05$. **(c)** Real-time PCR analysis of α5 subunit mRNA expression in rats injected with the Lenti-Control or Lenti-α5-shRNA virus into the hippocampus. Rats were euthanized ≥ three weeks after injection, and hippocampal microdissections were performed. Data are presented as mean (± SEM) fold change compared to the control mean (method of $2^{-\Delta\Delta CT}$); $t_{(4)}=2.6$, $p<0.05$. *$p<0.05$ versus control. **(d)** Data are presented as mean raw Ct values from the real-time PCR for the α5 assay and representative β-actin loading control in the habenula of rats.

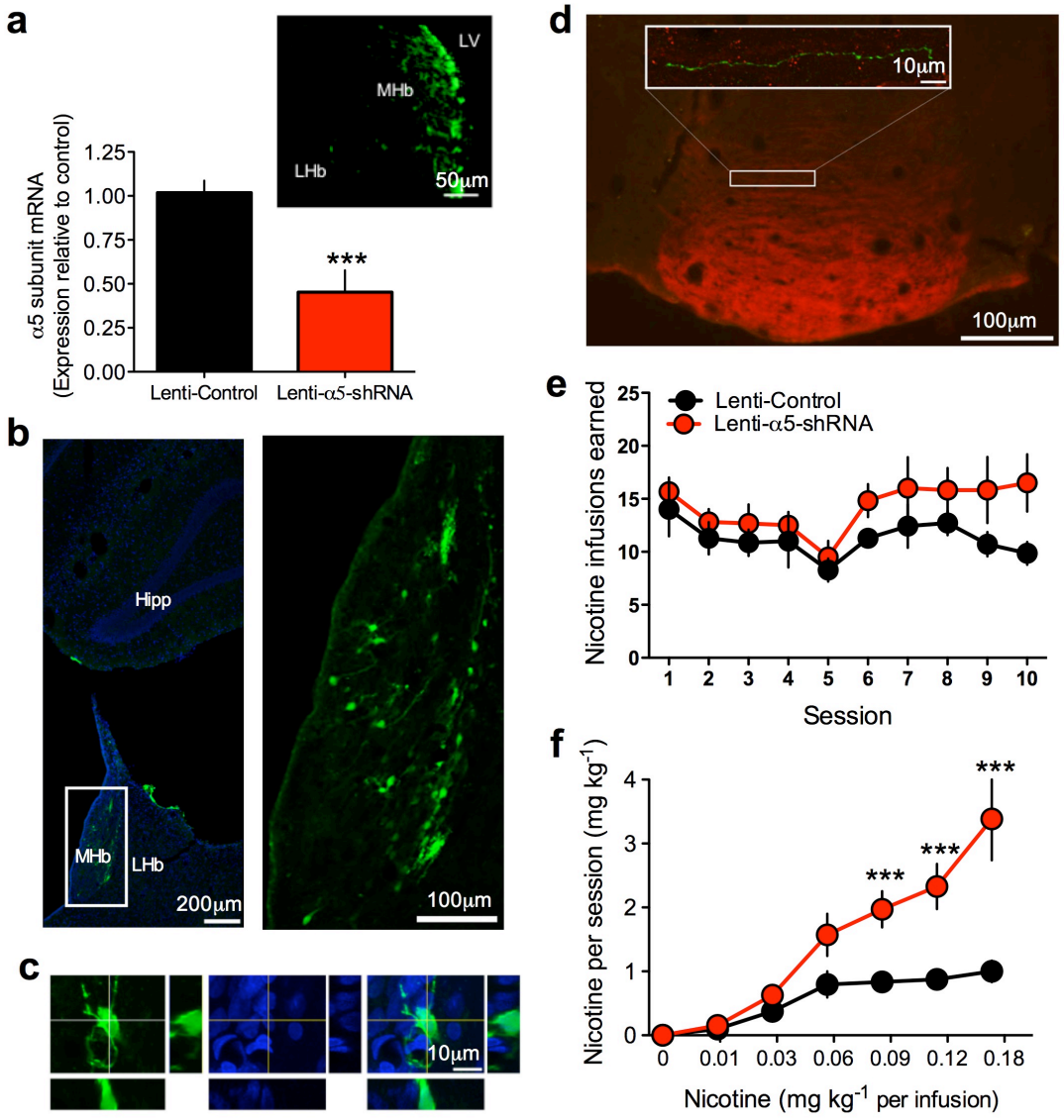

Supplementary Figure 10 | Lenti-α5-shRNA knockdown in the MHb of rats. (a) RT-PCR data depicting α5 mRNA expression in the MHb following injection of the Lenti-Control or Lenti-α5-shRNA virus in rats. Data are presented as mean (± SEM) fold change in α5 subunit mRNA levels; ***P<0.001. Insert: Representative GFP immunostaining highlighting virus-infected cells in MHb. **(b)** Additional representative images of GFP immunostaining in the MHb of rat. **(c)** High magnification images of a rat MHb neuron double labeled with GFP (green; left), DAPI (blue; center), and both markers (right). **(d)** GFP-positive axons were detected in the IPN of Lenti-α5-shRNA rats. **(e)** Rats acquired nicotine self-administration with the training dose (0.03 mg/kg/infusion) under a FR5TO20 sec schedule of reinforcement during 1 hr daily sessions (n=10-11/group). Data are presented as mean number of infusions earned ± SEM. Two-way ANOVA, *Lentivirus* $F_{(1,99)}$=4.08, n.s.; *Session* $F_{(9,99)}$=2.34, p<0.05; *Interaction* $F_{(9,99)}$=0.65, n.s. **(f)** Nicotine self-administration data from Fig. 3a (main manuscript) are presented as mean (± SEM) totals nicotine intake at each unit dose available. *Lentivirus* $F_{(1,60)}$=26.4, p<0.001; *Dose* $F_{(6,60)}$=38.2, p<0.0001; *Interaction* $F_{(6,60)}$=10.8, p<0.0001; **p<0.01, ***p<0.001, post-test after significant interaction effect.

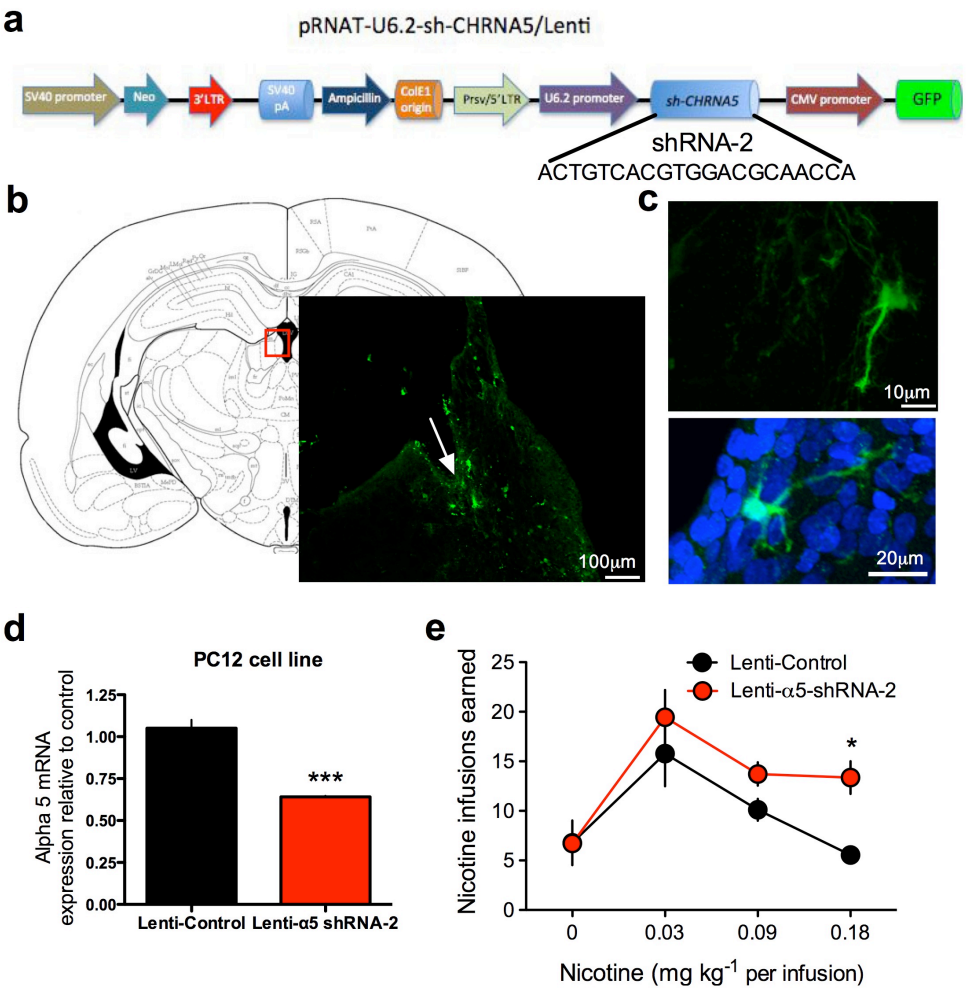

Supplementary Figure 11 | Validation of Lenti-α5-shRNA-2 knockdown vector and nicotine self-administration in rats. (a) Lentivirus vector map detailing construct. **(b)** Confocal image displaying injection site (arrow) and GFP-labeled cells (green) in the MHb of a treated rat. The schematic diagram illustrates location of displayed image (red box). Scale bar = 100 μm. **(b)** High magnification image displaying GFP-labeled cells and axons from the rat MHb. The bottom panel shows another cell with GFP and DAPI (blue) colabeling. Scale bars = 10 μm (top) and 20 μm (bottom). **(d)** Real-time PCR data for α5 subunit mRNA in PC12 cells at 24 hr post-transfection with the Lenti-Control or Lenti-α5-shRNA-2 vector. Data are presented as mean (± SEM) fold change compared to the untransfected control mean (method of $2^{-\Delta\Delta CT}$); $t_{(4)}$=8.07, ***p<0.001. **(e)** Rats were injected with the Lenti-Control or Lenti-α5-shRNA-2 virus in the MHb. After an incubation period of three weeks, the rats were implanted with IV catheters and trained to self-administer nicotine. Following the acquisition period, the unit dose available for nicotine self-administration was varied, and responding for nicotine infusions was assessed (*n*=9-11 per group). Data are presented as mean (± SEM) number of nicotine infusions earned. Two-way ANOVA: *Lentivirus* $F_{(1,54)}$=5.07, p<0.05; *Dose* $F_{(6,54)}$=13.97, p<0.0001; *Interaction* $F_{(6,54)}$=1.68, n.s. *P<0.05 versus Lenti-Control, post-hoc test.

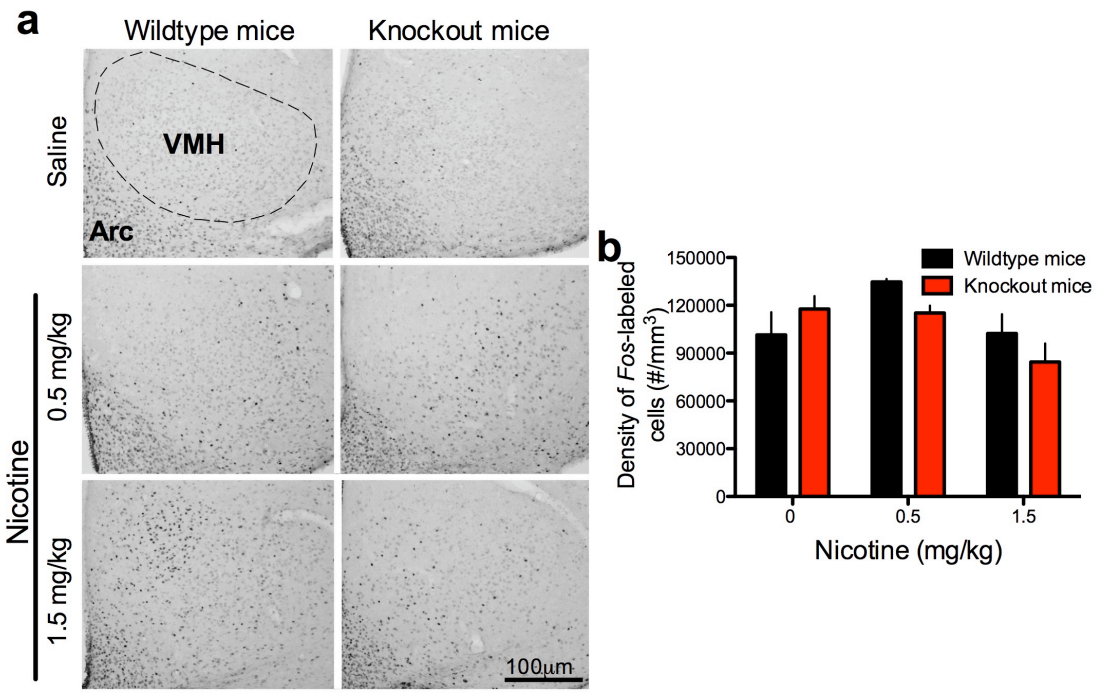

Supplementary Figure 12 | Expression of Fos immunoreactivity in the ventromedial hypothalamus (VMH). Fos staining in VMH was assessed in wildtype and α5 knockout mice (n=5/group) following subcutaneous injection of a moderate or high dose of nicotine (0.5 or 1.5 mg/kg, free-base) or saline. **(a)** Photomicrographs display Fos immunoreactivity in the VMH of wildtype (left panels) and α5 knockout (right panels) mice following saline (top panels), 0.5 mg/kg nicotine (center panels) or 1.5 mg/kg nicotine (bottom panels) injections. Scale bar = 100 μm. Arc: arcuate nucleus of the hypothalamus. **(b)** The density of Fos immunoreactive cells did not significantly differ among groups in the VMH. Data are presented as the mean (± SEM) density of Fos immunoreactive cells (number per mm^3). Two-way ANOVA, *Genotype* $F_{(1,24)}=0.78$, n.s.; *Drug* $F_{(2,24)}=5.18$, $p<0.05$; *Interaction* $F_{(2,24)}=2.12$, n.s.

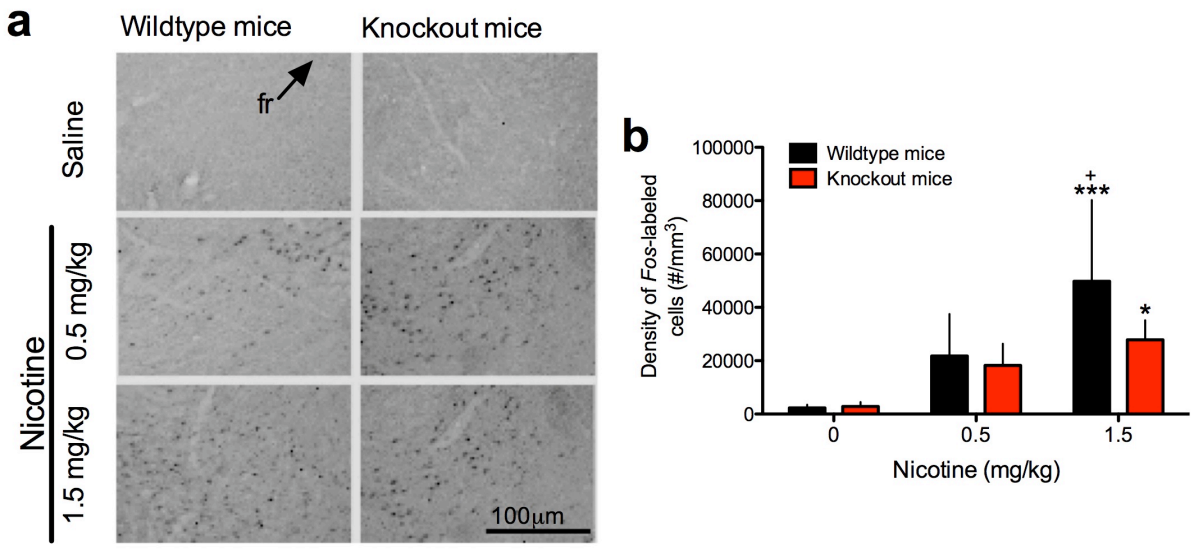

Supplementary Figure 13 | Expression of Fos immunoreactivity in the ventral tegmental area (VTA). Fos staining in VTA was assessed in wildtype and α5 knockout mice (n=5/group) following subcutaneous injection of a moderate or high dose of nicotine (0.5 or 1.5 mg/kg, free-base) or saline. **(a)** Photomicrograph of VTA showing Fos immunoreactivity. fr, fasciculus retroflexus. **(b)** Cell density in VTA was quantified with unbiased stereology. *Genotype* $F_{(2,24)}$=2.38, n.s.; *Drug* $F_{(2,24)}$=15.19, p<0.0001; *Interaction* $F_{(2,24)}$=1.67, n.s. *p<0.05 and ***p<0.001 indicate statistically significant difference compared to respective saline control. $^{+}$P<0.05 and $^{+++}$p<0.001 indicate statistical difference compared to respective 0.5 mg kg^{-1} nicotine group.

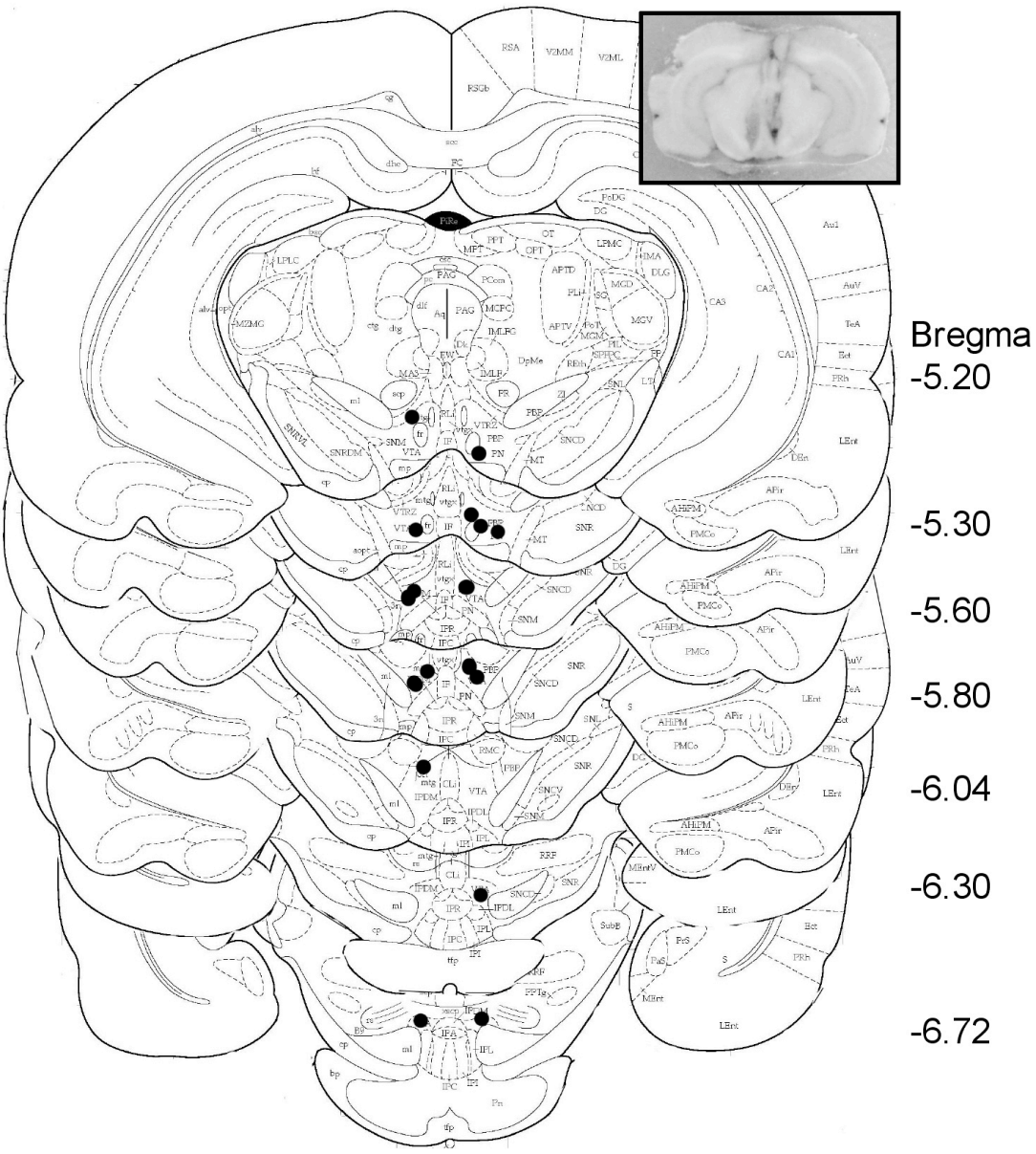

Supplementary Figure 14 | IPN injection sites for lidocaine, LY235959 and saline in rats. Injection sites were verified histologically for the IPN of all cannulated rats and are noted on the corresponding diagram plates. Insert: Image of representative injection tract into the IPN of a rat brain.

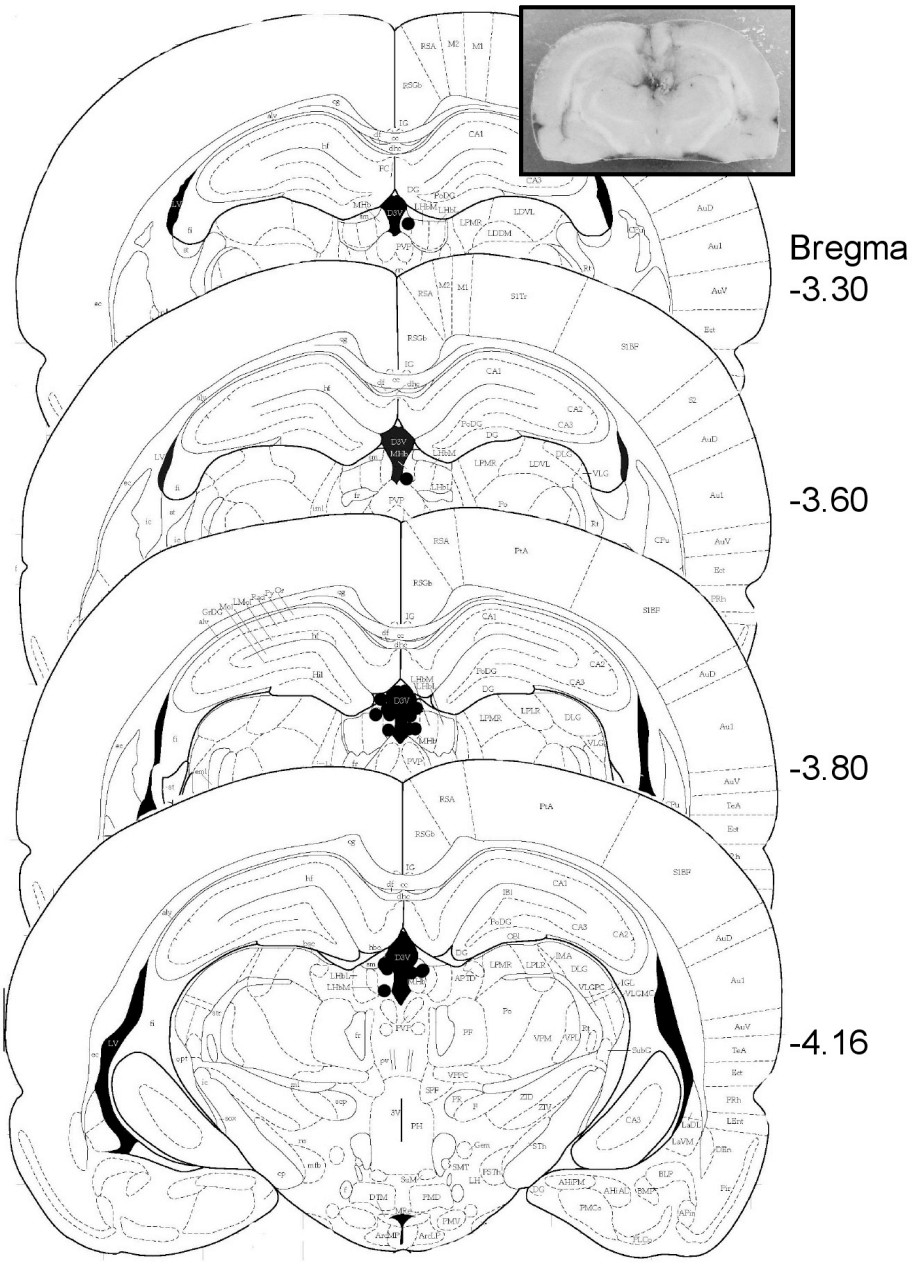

Supplementary Figure 15 | VTA injection sites for lidocaine, LY235959 and saline in rats. Injection sites were verified histologically for the VTA of all cannulated rats and are noted on the corresponding diagram plates. Insert: Image of representative injection tract into the VTA of a rat brain.

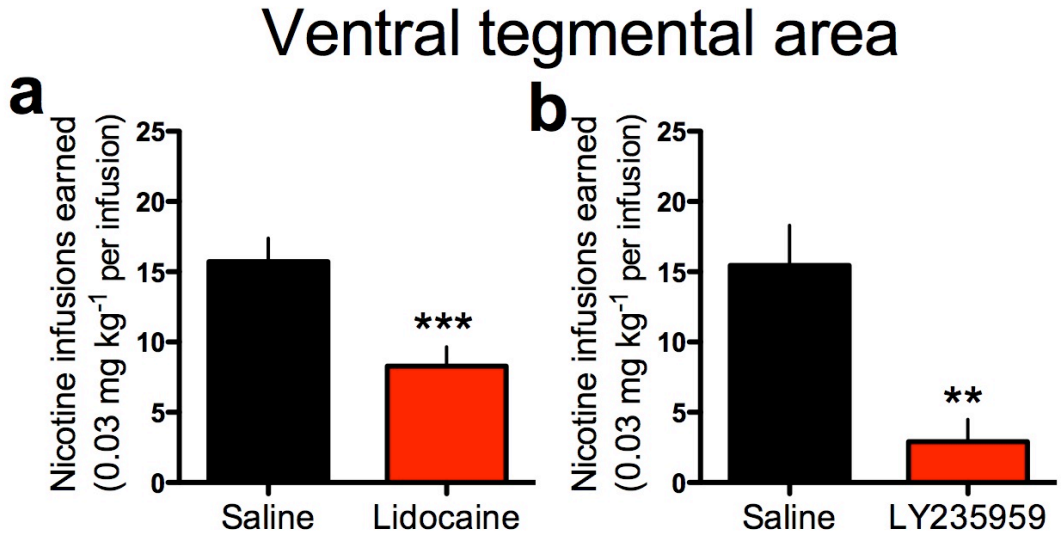

Supplementary Figure 16 | Disruption of VTA signaling decreases nicotine intake in rats. (a) Lidocaine-induced inactivation of VTA decreased nicotine intake in rats (n=11). T-test, $t_{(10)}$=4.60, ***p<0.001. **(b)** LY235959 (10 ng/side) infused into VTA decreased nicotine intake in rats (n=11). T-test, $t_{(10)}$=3.90, **p<0.01. Data are presented as mean (± SEM) number of nicotine infusions earned.

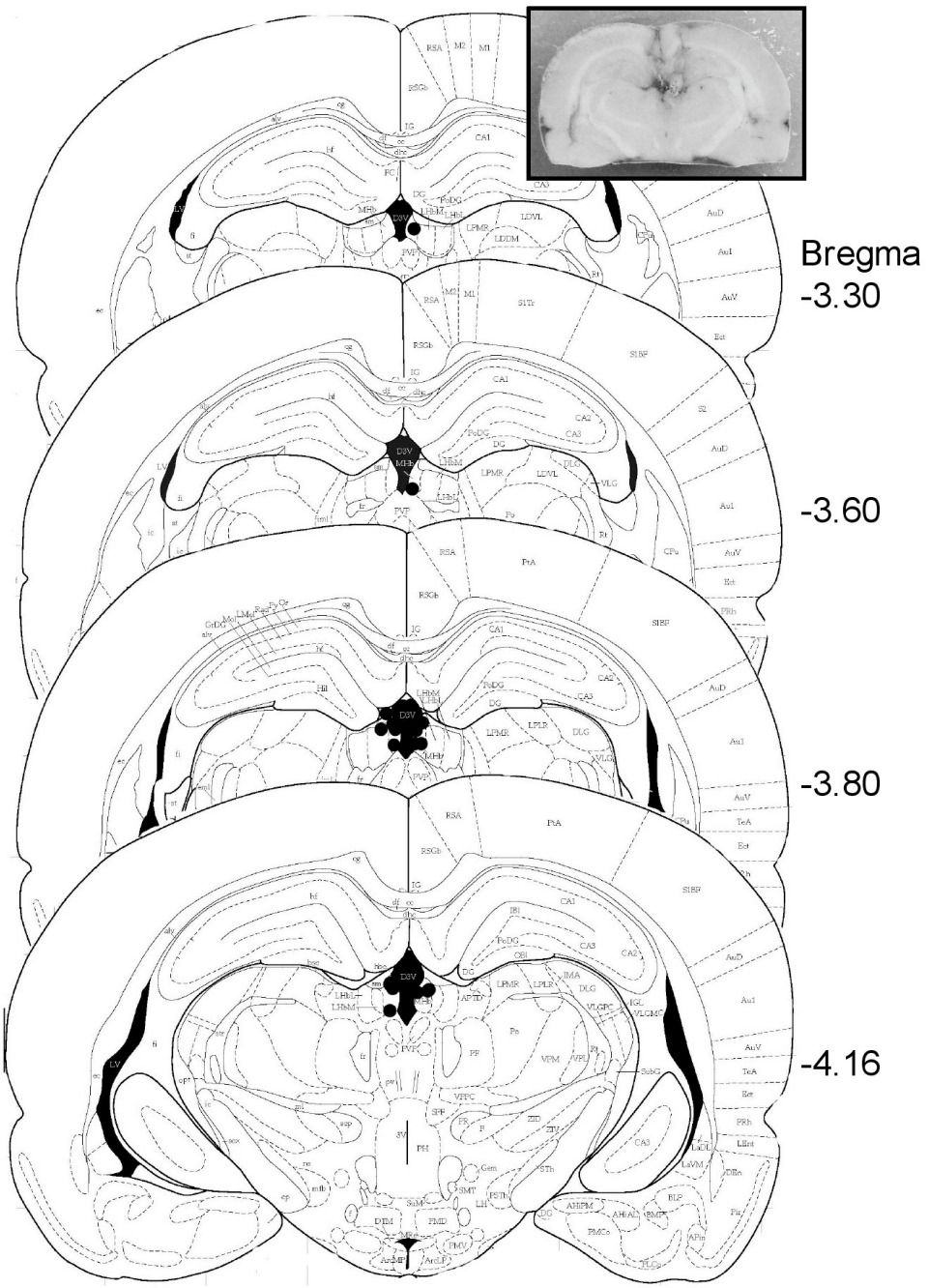

Supplementary Figure 17 | Medial habenular (MHb) injection sites for lidocaine, LY235959 and saline in rats. Injection sites were verified histologically for the MHb of all cannulated rats and are noted on the corresponding diagram plates. Insert: Image of representative injection tract into the MHb of a rat brain.

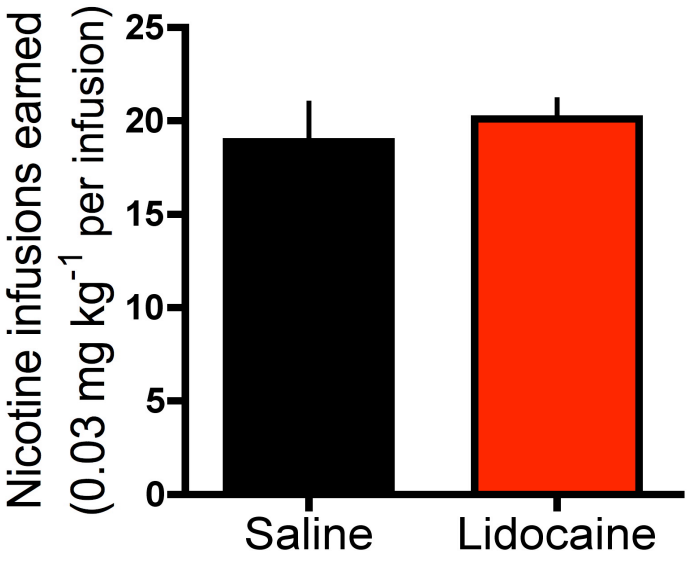

Supplementary Figure 18 | Lidocaine-induced reversible lesions of the MHb on nicotine intake in rats. Microinjections of lidocaine into the MHb did not alter nicotine self-administration at the 0.03 mg/kg/infusion nicotine dose in rats (n=9). Data are presented as mean (± SEM) number of nicotine infusions earned; t-test, $t_{(8)}$=0.44, n.s.

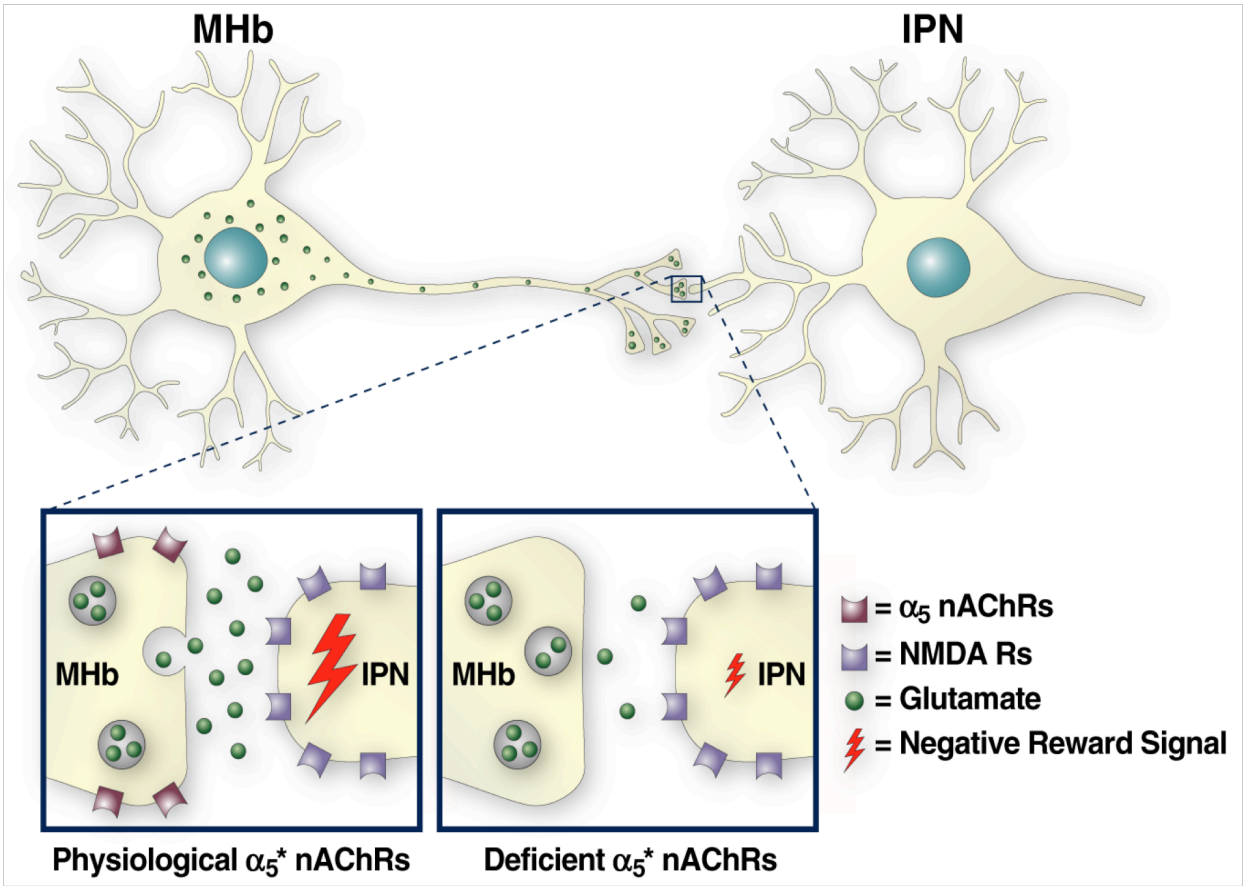

Figure 19 | Proposed mechanism through which α5* nAChRs control nicotine intake. Representation of an MHb neuron projecting to IPN and expressing presynaptic α5* nAChRs. Nicotine consumption stimulates the MHb-IPN pathway through α5* nAChRs, thereby increasing excitatory glutamatergic transmission and subsequent NMDA receptor activation in IPN. High levels of IPN activity elicit an inhibitory motivational signal that decreases motivation to further consume nicotine. Deficits in α5* nAChR signaling decreases sensitivity of the habenulo-interpeduncular pathway to nicotine, consequently attenuating IPN-derived inhibitory motivational signals that moderate nicotine intake.